Acute Exposure of Upcyte® Hepatocytes to Sub-lethal Concentrations of Graphene Oxide: Impairment of Phase-I Xenobiotic Metabolism and Albumin Transcription

Alessio Romaldini
Istituto Italiano di Tecnologia
Raffaele Spanò
Istituto Italiano di Tecnologia
Stefania Sabella (stefania.sabella@iit.it)
Drug Discovery and Development Department, Istituto Italiano di Tecnologia, via Morego 30, 16136, Genoa, Italy https://orcid.org/0000-0003-3353-3607

Research

Keywords: graphene oxide, hepatocytes, liver, xenobiotic metabolism, cytotoxicity, apoptosis, oxidative stress, inflammation, cytochrome P450, albumin

Posted Date: January 18th, 2021

DOI: https://doi.org/10.21203/rs.3.rs-147026/v1

Abstract

Background

Graphene Oxide (GO) is a promising candidate for nanomedicine applications. Due to the central role of liver in biotransformation of xenobiotics and drugs, the impact of GO on hepatic functional cells represents a crucial evaluation step for its potential implementation as drug. Primary human hepatocytes (PHH) are the election model for studying drug toxicity and metabolism, however current technical limitations may slow down the large-scale diffusion of this cellular tool in *in vitro* investigations. To assess the potential hepatotoxicity of GO, in this study, we propose an alternative approach employing second-generation upcyte® hepatocytes as cell model, which show metabolic and functional profiles akin to PHH. Cells have been acutely exposed to increasing GO concentrations for 24 hours. Upon sub-lethal concentrations of GO, stress-related cell responses to GO (such as apoptosis, oxidative stress and inflammatory response) have been evaluated, along with a broad investigation of GO impact on specialized hepatic functions.

Results

Results show an IC_{50} equal to 102.2 µg/mL, which is in line with recent data obtained by hepatocellular carcinoma-derived cells. However, at sub-lethal doses (≤ 80 µg/mL), it is detected a mild activation of early apoptosis, but not oxidative stress or inflammatory response. Importantly, we observed a clear impact of GO on phase-I drug metabolism enzymes (*e.g.,* CYP3A4, CYP2C9) through the inhibition of gene expression and metabolic activity. Conversely, phase-II enzyme system and phase-III efflux transporters were not affected by GO. Finally, GO strongly downregulated the gene expression of Albumin.

Conclusion

The presented model of upcyte® hepatocytes appears to be feasible for the assessment of hepatotoxicity of nanomaterials, specifically showing that sub-lethal doses of GO have a negative impact on the specialized hepatic functions of these cells. The impairment of cytochrome P450 system along with the alteration of Albumin gene expression by GO may suggest potential detrimental consequences for human health, as for instance, an altered detoxification from xenobiotics and drugs.

Introduction

Graphene is a carbon-based material consisting in a single layer of sp^2-hybridized carbon atoms arranged in two-dimensional (2D) honeycomb-shaped lattice [1]. In the last decade, graphene and its derivatives have been raising huge interests in many industrial fields (*e.g.*, electronics, energy storage or thermal isolation) owing to their peculiar physical-chemical characteristics. In particular, graphene oxide (GO) is a promising nanomaterial for nanomedicine applications [2], including drug and gene delivery, bioimaging and tissue engineering [3]. GO is commonly obtained via graphite oxidation and its chemical structure is characterized by the presence of highly reactive oxygenated chemical functional groups, such

as epoxy, hydroxyl and carboxyl groups [4, 5]. These functionalities make GO water-soluble and easily conjugable to bio-macromolecules or small ligands. Therefore, for such intrinsic properties, GO can be considered a suitable candidate for loading drugs or other bioactive molecules and/or for acting as vehicle system of drugs. However, the potential technological boost of GO raises concerns related to its safety for human use [6]. In the development of innovation technological processes of GO as novel drug, the early application of toxicology tools may be useful to predict toxicity at an early stage of the material design and development, thus offering a rapid safety screening for many combinations of GO-based materials. This approach requires the quick identification of dose-limiting toxicities (*e.g.*, sub-lethal doses), along with the material impact on organ specific functionalities (*e.g.*, hepatotoxicity). Furthermore, it possibly requires the application of *in vitro* models accounting for human body compartments (*e.g.*, gastrointestinal tract, lung, liver, spleen, and so forth), due to their central role in drug pharmacokinetic (*i.e.*, administration, distribution, metabolism and elimination [6]). *In vivo* studies on bio-distribution reported that, after entering the blood stream (through primary or secondary routes), GO may accumulate in many organs including liver, where interactions with liver functional cells may be likely [7–10]. Indeed in mouse models, it is evidenced an early degeneration and necrosis of hepatocytes in proximity of central vein [8] and the activation of IL-6 gene expression in parenchymal hepatocytes [10], upon animal exposure to GO. Data also indicate that, despite GO can be eliminated from the body via faeces and/or urine [7, 8, 11, 12], it behaves as a bio-persistent material in both human relevant simulated biological fluids (*e.g.*, gastro-intestinal fluid [13]) and epithelial *in vitro* models (such as gut and lung [13, 14]). Moreover, on the side of *in vitro* investigations, recent studies (which mostly employ hepatocellular carcinoma-derived cells) have indicated an IC_{50} approximately within the range of 50 and 100 μg/mL GO [15, 16]. Although the useful information gathered by these *in vitro* models, however, it emerges a knowledge gap about GO impact on specialized hepatic functions (such as phase-I and II drug metabolism enzymes, phase-III efflux transporters and Albumin), which, among many others, are useful descriptors for an early safety assessment of a nanomaterial in the innovation process. In fact, the above-mentioned models show a very low gene expression and a reduced metabolic activity of xenobiotic-metabolizing enzymes [17]. Based on their metabolic and functional features, primary human hepatocytes (PHH) represent the gold standard especially for studying drug metabolism and toxicity, but their limited availability and technical drawbacks greatly hamper their use at large scale [18, 19]. To avoid these limitations, in the present study we propose an alternative approach using proliferating, differentiated human hepatocytes generated using upcyte® technology, since hepatic functionalities (phase-I and -II enzymes gene expression, cytochromes P450 metabolic activity, Albumin production) and toxicological responses are similar to those of PHH [17, 19, 20]. These cells were obtained from PHH, after transduction with HPV *E6* and *E7* genes followed by positive selection of slowly proliferating OSM-responsive cells [19]. As a result, they are not immortalised, present a normal karyotype and do not display a transformed phenotype. Therefore, upcyte® hepatocyte cultures may have the capacity to display GO *in vitro* toxicity and/or its potential impact on hepatocyte metabolism and functions. In our investigations, 2D cultures of upcyte® hepatocytes were acutely exposed to increasing concentrations of GO in order to evaluate their potential effects on cell viability, apoptosis activation, inflammatory response, oxidative stress induction and, finally, hepatocyte-specific functions. To the best of our

knowledge, no data are currently available about the assessment of GO cytotoxicity in human differentiated, functional hepatocytes. Consequently, our study provides a piece of information on GO hepatotoxicity *in vitro*, related not only to cell viability but also to functionalities of hepatocytes.

Results

Characterization of GO in Milli-Q® water and in complete HHPM

GO used in our investigations showed the typical flake-like shape, as revealed by scanning electron microscopy (**Figure S1A**, *Supplementary Material*). This data is in line with previously reported observations [13]. To measure the hydrodynamic size, GO was dispersed in either Milli-Q® water or complete HHPM using increasing concentrations (4, 20, 80 µg/mL) and different incubation times (0, 2 and 24 hours; Fig. 1A). Results show that after 2 hours of incubation in complete HHPM, 4 µg/mL GO suspension presents three main peaks with a relative mean size of 7.9 nm ± 0.1 nm (peak #1), 338.9 nm ± 29.0 nm (peak #2) and 5131.4 nm ± 274.8 nm (peak #3), respectively. As shown in **Figure S1B** (*Supplementary Material*), the smaller peak (peak #1) is identified and likely refers to the protein components supplemented in complete HHPM [22]. Peaks #2 and #3 are, therefore, relative to two GO populations, with peak #2 that, based on its relative intensity (73.1%), corresponds to the most representative size population. Instead, peak #3 is indicative of partial GO agglomeration/aggregation, which is quite similar in both the dispersants used. As the GO concentration increases (20–80 µg/mL), it is noticed a very slow shift of peak #2 toward larger sizes in both complete HHPM and Milli-Q® water along with a progressive rise of the relative peak intensity. Overall, these data suggest that the suspension is poly-dispersed, having a mild tendency to agglomerate/aggregate. However, such effect does not increase after a longer time of incubation as no changes in terms of hydrodynamic size and intensity are observed after 24 hours of incubation in complete HHPM. The tendency to agglomerate/aggregate of GO at higher concentrations (20–80 µg/mL) is also evidenced by the presence of a sediment, as reported in Fig. 1B. Peak position and relative intensity of all the peaks identified in each tested condition are reported in **Table 2** (*Supplementary Material*). The zeta potential analysis shows a negative surface charge of GO in Milli-Q® water, which goes from − 35 mV to -41 mV as a function of the concentrations applied (Fig. 1C). After 24-hour incubation in complete HHPM, the surface charge of GO increased to about − 27.5 mV, as a consequence of the possible formation of a bio-macromolecular corona around GO [22]. The particle-corona complexes (see technical details in Materials and Methods) show mean hydrodynamic diameters quite comparable to those of bare GO (**Figure S1C** and **Table 2**, *Supplementary Material*).

GO impacts on cell viability and exerts membrane damage in upcyte® hepatocytes

To understand the possible detrimental impact of GO on upcyte® hepatocytes, we first evaluated its impact on cell viability and cell membrane integrity. Confluent cell cultures were treated for 24 hours with increasing GO concentrations, as reported in Fig. 2A. A wide concentration range (4-320 µg/mL) was applied to calculate the half maximal inhibitory concentration (IC_{50}). As evidenced by the reduction of the metabolic activity, GO determined a dose-dependent reduction of cell viability, with an IC_{50} equal to 102.2 µg/mL (Fig. 2A). Note that, the highest GO concentration tested, corresponding to 320 µg/mL, caused a cell viability reduction comparable to the lethal effect exerted by the positive control, which was 0.03% Triton X-100 (**Figure S2A**, *Supplementary Material*). As revealed by the cytotoxicity assay, treated cells also showed a significant release in the culture medium of the cytosolic lactate dehydrogenase (LDH), indicating a clear cytotoxicity due to cell membrane damage (Fig. 2B). In particular, it is possible observing a significant increase of cytotoxicity with respect to the control condition to about 11.5% ($p = 0.0015$) at 80 µg/mL GO, a concentration value lower than the IC_{50}, whereas at lethal doses (320 µg/mL), the damage weakly increased only up to 17% ($p < 0.0001$). In addition, with the increase of GO concentration, the decrease of cell viability alongside the increase of released LDH showed a significant negative linear correlation ($p < 0.0001$ and Pearson's $r = 0.9521$; **Figure S2B**, *Supplementary Material*). The morphology analysis confirmed cytotoxicity results, revealing that, with the increase of GO concentration (starting from 80 µg/mL GO), cells showed an evident morphological change along with a size reduction. Conversely, control cells were characterized by normal spreading round shape (Fig. 2C). The progressive GO deposition on the top surface of treated cells, especially at concentration values higher than IC_{50} (102.2 µg/mL), was observed. This phenomenon is indicative of a partial colloidal instability of GO suspensions (as evidenced also by DLS analysis), so mechanical cell damage due to particle deposition cannot be excluded.

GO induces early apoptosis but not oxidative stress and inflammatory response in upcyte® hepatocytes at sub-IC_{50} doses

To assess if GO induces apoptosis, oxidative stress or inflammation in upcyte® hepatocytes, cells were treated with increasing sub-IC_{50} doses of GO (2–80 µg/mL). Regarding apoptosis induction, we screened the extent of phosphatidylserine (PtdSer) exposure over time by treated cells (Fig. 3A). At the first hours (3 and 6 hours) of GO stimulation, no significant variation of PtdSer was observed at any of tested concentrations. However, after 24 hours of treatment, PtdSer exposure significantly increased about 1.29-folds with respect to the control, upon treatment with 20 µg/mL GO ($p = 0.0352$). This increment remained almost unvaried at higher concentrations (40 µg/mL GO, $p = 0.0043$; and 80 µg/mL GO, $p = 0.0429$). It is important to underline that GO showed just mild induction of PtdSer exposure and a different kinetic in comparison to the positive control (0.5 µM Staurosporine). Indeed, Staurosporine induced an earlier significant increase of PtdSer exposure, reaching a maximum peak at 6 hours ($p < 0.0001$). PtdSer level reached again the basal value after 24 hours of Staurosporine treatment in correspondence to the appearance of necrotic cells (**Figure S3**, *Supplementary Material*). To evidence signs of cellular apoptosis, the intracellular amount of cleaved-PARP in GO-treated cells was also measured. We found no alteration of cleaved-PARP levels, with respect to the control, at any of tested concentrations, further confirming the

mild effect induced by GO (Fig. 3B). Since oxidative stress is involved in many mechanisms of cytotoxicity (such as apoptosis, DNA damage, lipid peroxidation), we investigated the possible role of GO as oxidative stress inducer [30]. We found that GO did not modulate the gene expression of the two main cellular antioxidants, HO-1 and SOD1, at any of tested concentrations (Fig. 3C). As opposite, the positive control (400 μM H_2O_2) induced a significant upregulation of HO-1 and SOD1 gene expression ($p = 0.0094$ and $p = 0.0269$, respectively). Upon GO treatment, western blot analysis of HO-1 and SOD1 confirmed the absence of significant variations of the corresponding protein levels with respect to the control (Fig. 3D). As far as inflammatory response is concerned, GO did not induce modification in the gene expression of TNFα, IL-1β, IL-6 and IL-8, considered as mediators of inflammation (Fig. 3E). As opposite, upcyte® hepatocytes treated overnight with complete medium supplemented with 100 μg/mL LPS (positive control) showed a significant upregulation of gene expression of IL-1β, IL-6 and IL-8 ($p = 0.0482$, $p < 0.0001$ and $p = 0.0001$, respectively).

GO impairs cytochrome P450 system in upcyte® hepatocytes at sub-lethal concentrations

To evaluate the GO impact on cytochrome P450 system of upcyte® hepatocytes, cells were treated for 24 hours with increasing sub-IC_{50} doses (2–80 μg/mL). We measured the gene expression and the corresponding metabolic activity of CYP3A4 and CYP2C9, which are the most representative enzymes of that system. In parallel, the responsiveness of cytochromes P450 was assessed making use of well-known drugs. For this aim, cells were daily incubated up to 72 hours [28, 29] with 50 μM Rifampicin or 100 μM Ciprofloxacin, which act as inducer and inhibitor of both CYP3A4 and CYP2C9, respectively. Results show that, upon treatment with Rifampicin, CYP3A4 gene expression was about 41-folds upregulated with respect to un-treated cells ($p = 0.0052$; Fig. 4A, upper panel), whereas, when cells were treated with Ciprofloxacin, 0.6-folds downregulated in comparison to the control level ($p = 0.0138$; Fig. 4B, upper panel). Similarly, CYP2C9 gene expression was significantly regulated upon the same treatments, with a Rifampicin-mediated upregulation of about 4.0-folds ($p = 0.0047$; Fig. 4D, upper panel) and a Ciprofloxacin-mediated downregulation to about 0.7-folds with respect to un-treated cells ($p = 0.0444$; Fig. 4E, upper panel). Moreover, we evaluated the metabolic activity of CYP3A4 and CYP2C9 using as substrates two fluorescent compounds, 7-benzyloxy-4-trifluoromethylcoumarin (BFC) and 7-methoxy-4-trifluoromethylcoumarin (MFC), respectively. Results indicate that the activity of CYP3A4 was statistically increased of about 290% in Rifampicin-treated cells with respect to the control ($p = 0.0247$; Fig. 4A, lower panel), whereas it appeared to be reduced to about 64% in the case of Ciprofloxacin-treated cells ($p = 0.0006$; Fig. 4B, lower panel). Comparably, CYP2C9 activity was modulated by the same treatments consistently with gene expression regulation (Fig. 4D **and E**, lower panels). Afterwards, we evaluated the effect of sub-IC_{50} concentrations of GO on cytochrome P450 system. We observed a dose-dependent downregulation of CYP3A4 gene expression (starting from 4 μg/mL, $p = 0.0015$), which was equal to about 0.37-folds with respect to the control level at the highest concentration (80 μg/mL GO, $p < 0.0001$; Fig. 4C, upper panel). Consistent with the gene expression, CYP3A4 metabolic activity showed a significant and progressive dose-dependent reduction, reaching a level of about 18.6% with respect to the

control, at concentration value of 80 µg/mL GO ($p = 0.0002$; Fig. 4C, lower panel). In parallel, CYP2C9 gene expression significantly decreased starting from 20 µg/mL GO ($p = 0.0012$), down to about 1.9% with respect to the control level with 80 µg/mL GO ($p < 0.0001$; Fig. 4F, upper panel). CYP2C9 metabolic activity was also significantly reduced, reaching about 10.9% of the basal level with the highest GO concentration (80 µg/mL, $p = 0.0006$; Fig. 4F, lower panel). For both CYP3A4 and CYP2C9, GO-mediated gene expression downregulation had a significant positive linear correlation with the metabolic activity impairment ($p = 0.0119$ and Pearson's $r = 0.9095$ for CYP3A4 and $p = 0.0015$ and Pearson's $r = 0.9682$ for CYP2C9; **Figure S4A and B**, *Supplementary Material*). Our results indicate a strong inhibition activity of GO on CYP3A4 and CYP2C9 gene expression and relative metabolic activities. Such an inhibitory response appears to be dose-dependent and the negative effect of 4 µg/mL GO could be approximately compared to that induced by 100 µM Ciprofloxacin (~33 µg/mL). The inhibition of cytochrome P450 system by sub-lethal doses of GO was confirmed also on CYP2B6 and CYP1A2 (**Figure S4E and H**, *Supplementary Material*). For CYP2B6, gene expression decreased starting from 20 µg/mL GO ($p = 0.0069$), while GO affected CYP1A2 gene expression at lower doses (2 µg/mL; $p = 0.0052$). Upon 80 µg/mL GO treatment, CYP2B6 and CYP1A2 reached a gene expression equal to about 4.3% and 11.3% of the control level ($p < 0.0001$ for both), respectively. In contrast to the effects exerted on CYP3A4 and CYP2C9 gene expression, Rifampicin and Ciprofloxacin had no effects on CYP2B6 and CYP1A2, revealing their specific mechanism of action only on CYP3A4 and CYP2C9 in upcyte® hepatocytes (**Figure S4C, D** and **S4F, G**, *Supplementary Material*). Conversely, GO seems to act on a wide range of targets within cytochrome P450 system.

GO does not modulate gene expression of phase-II GST and phase-III ABCG2, but downregulates expression of Albumin

After having observed the effects of GO on phase-I drug metabolism enzymes, we investigated the effect of sub-lethal GO exposures on phase-II and phase-III drug metabolism/transport enzymes in upcyte® hepatocytes. In particular, the gene expression of Glutathione S-Transferase (GST) and ATP Binding Cassette Subfamily G Member 2 (ABCG2) was evaluated. Results show that GST and ABCG2 gene expression was not modulated by GO at any concentration tested (Fig. 5A **and B**). After that, we investigated the effect of GO on the gene expression of two xenobiotic-sensing receptors, *i.e.*, PXR and CAR (**Figure S5A and B**, *Supplementary Material*), finding that GO significantly downregulated PXR gene expression to about 12% with respect to the control level only at 80 µg/mL ($p = 0.0224$), whereas it was ineffective on CAR gene expression at all tested concentrations. Finally, we analysed the gene expression of Albumin, finding that Albumin was statistically, dose-dependently downregulated to about 5.2% with respect to the control level with 80 µg/mL ($p < 0.0001$; Fig. 5C).

Discussion

This study aimed at investigating *in vitro* hepatotoxicity of GO after 24-hour acute exposure in a 2D-cell culture model of second-generation upcyte® hepatocytes. These cells represent an interesting model, since they are generated from primary human hepatocytes (PHH) via genetic engineering in order to

induce the expression of HPV *E6* and *E7* genes [20]. Second-generation upcyte® cells are derived from *E6/E7*^{low} cell colonies, which are slowly proliferating cells, able to proliferate upon treatment with OSM (IL-6-like protein) and to differentiate terminally in 4 days after OSM removal [19]. These cells are not immortalised, have a normal karyotype and are metabolically and functionally similar to differentiated PHH [19, 20, 31]. In addition, cells applied in this study are derived from the specific donor 653-03, which apart the good basal activity of cytochromes P450 (CYPs), shows also an appropriate responsiveness to known inducers and inhibitors of CYP enzymes [31]. Based on these features, upcyte® hepatocytes may resemble the functionality of primary hepatocytes and then can be considered a reliable *in vitro* cell culture model for studying the acute effects induced by toxicants on the hepatic tissue. In this study, we focused our attention on GO, which, together with other nanomaterials belonging to the wider family of graphene, has raised great interests due to its potential in nanomedicine. However, hazard assessment, focused on human health, is required for a safe development of these materials [6, 32]. To this regard, in view of medical applications, it then appears clear how important is the understanding of the potential impact of GO on hepatic tissue, since liver has a central role in the biotransformation and detoxification of xenobiotics, after their entrance in the circulatory system. Before the *in vitro* cellular study, GO was characterized in terms of morphology, lateral dimensions and surface charge by SEM, DLS and Zeta Potential analysis. When dispersed in Milli-Q® water, GO showed the typical flake-like structure of graphene, size distribution (about 300 nm) and a surface charge (from − 35 mV to -41 mV) comparable to data previously published [13]. In complete HHPM, GO adsorbed medium proteins [22] and had an appreciable tendency to sediment, possibly related to the increased surface charge (-27.5 mV). We focused on acute toxicity of increasing concentrations of GO (4-320 µg/mL) using a 24-hour exposure of upcyte® hepatocytes. By applying such a wide concentration range, we found an IC_{50} equal to 102.2 µg/mL along with relevant cytotoxic effects (such as morphological changes, cell membrane damage and cell viability reduction) at concentrations higher than 80 µg/mL. This data appears to be in line with those obtained with HepaRG™ cell line, which, although with some differences, presents hepatocyte-like differentiated phenotype [33, 34]. These cells, upon treatment with 50 µg/mL GO, showed indeed absence of toxicity [35]. Noteworthy, to the best of our knowledge, this is the only work which investigated the potential toxicological effect of GO using a cell line presenting features comparable to human hepatocytes, even though it is an organotypic co-culture of hepatocyte- and cholangiocyte-like cells, as opposite to upcyte® hepatocytes. Overall, our results indicated a GO-mediated toxicity at a concentration range also comparable to immortalized cell lines. HepG2 cells, when treated with GO, presented an IC_{50} approximately within the range of 50 and 100 µg/mL along with a clear cell viability reduction at concentration values higher than 80 µg/mL [15, 16]. In L02 cells, GO provoked only a moderate cell viability reduction at 100 µg/mL or higher concentrations [36]. Taken together, these data indicate that the toxicological responses on hepatic cells induced by GO treatments seem not particularly affected by the cell type intrinsic features. Afterwards, we studied stress-related cell responses (apoptosis, oxidative stress and inflammation) in upcyte® hepatocytes upon acute treatment with increasing sub-IC_{50} doses of GO (2–80 µg/mL). In the range of 20–80 µg/mL GO, we found an increased temporal exposure of PtdSer, but unvaried protein levels of cleaved-PARP. PtdSer is normally present in the inner layer of plasma membrane, but it is exposed to the outer layer as “eat me” signal for macrophages during

apoptosis [37]. In normal conditions, PARP is involved in DNA repair, but, when it is proteolytically cleaved by the executioner Caspase-3, the apoptotic process is irreversible [38, 39]. Based on these mechanisms, the obtained results indicate an early-stage induction of apoptosis by GO, which does not undergo to maturation (no cell death in upcyte® hepatocytes at the end of the treatment, according to no changes in cleaved-PARP levels). Similarly, it has been reported a dose-dependent increase of early apoptotic cells after 24 hours of GO treatment, both in L02 cells [36] and in HepG2 cells [15], even though higher GO doses were used with L02 cells (100 and 300 μg/mL) with respect to HepG2 cells (up to 50 μg/mL). Moreover, Chatterjee et al. reported that apoptosis executioners (Caspase-8, -9 and − 3) were un-affected or even downregulated after 24 hours of treatment with both 20 μg/mL and 81 μg/mL of GO, showing that late apoptotic cells increased in number only after longer treatments (48 hours) [15]. In relation to intracellular antioxidant defences in upcyte® hepatocytes, we found no modulation of both gene expression and protein levels of cellular antioxidants HO-1 and SOD1 after 24 hours of GO treatment, suggesting that GO should have induced no or weakly the generation of endogenous reactive oxygen species (ROS). However, some recent studies show ROS generation after different times of exposure in both HepG2 cells and L02 cells, with differences in treatments and collection times [15, 16, 36, 40]. Notably, upcyte® hepatocytes could be less susceptible to GO-induced oxidative stress in comparison with immortalized hepatic cells or their antioxidant defenses could be sufficient to neutralize a mild generation of ROS. Finally, we evaluated the inflammatory response of upcyte® hepatocytes upon GO treatment, showing no pro-inflammatory response (none of four tested mediators was altered, at the experimental conditions applied in the study). Conversely, using immortalized hepatic cells (HepG2 cells), Liu et al. reported a significant upregulation of IL-6 gene expression upon 24-hour exposure to 5 μg/mL GO [16], whereas, upon 24-hour stimulation with 20 μg/mL GO, Chatterjee et al. observed changes in inflammatory gene expression, possibly mediated by TGFβ1 signalling [15]. A similar pro-inflammatory response was observed both *in vitro* and *in vivo* by Zhang et al. [10]. Different size GO (small-GO, range 50–200 nm; medium-GO, range 200–500 nm; and large GO, range 500–2000 nm) enhanced IL-6 gene expression and secretion by different hepatic cell lines (Hepa1-6, HepG2 and Huh7 cells). *In vivo*, intravenous injection of different sized GO in the IL-6 reporter mouse model showed an increase of IL-6 expression, specifically in liver, by activation in parenchymal cells. IL-6 induction was directly dependent both by GO concentration and size. Moreover, a weak pro-inflammatory response was detected in a 3D airway model (primary human bronchial epithelium), sub-chronically treated with increasing concentration of aerosolized GO [14]. By contrast, Lee et al. demonstrated *in vivo* that GO polarized invariant natural killer T-cells towards an anti-inflammatory phenotype, dampened pro-inflammatory cytokine production and protected mice against liver injuries due to induced inflammatory responses [41]. Similarly, Han et al. reported that GO attenuated inflammation by the modulation of the polarization of mouse macrophages [42]. Based on these experimental evidence, it seems that GO could act as a pro- or an anti-inflammatory stimulus, depending on the size, the actual concentration applied, the oxidation status of the surface and the targeted cell type. Overall, these data indicate that GO was not toxic for upcyte® hepatocytes, when acutely administered in a sub-lethal range. In the second part of this study, we focused our attention on two main hepatocyte-specific functions, such as drug metabolism/transport and Albumin production, taking advantage by peculiar features of upcyte® hepatocytes. Regarding the

metabolism of xenobiotics/drugs, cytochromes P450 represent the most important phase-I enzymes in human functional hepatocytes [43]. For the presented study, we selected as representative enzymes and potential GO targets some CYPs (CYP3A4, CYP2C9, CYP2B6 and CYP1A2), which are the most abundant enzymes involved in biotransformation reactions of liver. Results show that, at sub-lethal doses, GO dose-dependently downregulated all tested CYPs. For CYP3A4 and CYP2C9, the effect of inhibition was demonstrated also for the enzyme metabolic activities, suggesting either a direct inhibitory effect of GO or a reduced amount of such enzymes caused by the reduced corresponding transcription. Such findings reinforced the preliminary evidence of GO inhibition effects on cytochrome P450 system reported by Strojny et al. [35]. In that work, although using different *in vitro* approaches (such as the differentiated HepaRG™ cells for monitoring CYP gene expression and a microsomal-based model for assessing CYP metabolic activity), it has been reported a strong reduction of transcription of many CYP isoforms (CYP3A4, CYP2B6, CYP1A2 and CYP2E1) and the inhibition of the catalytic activity of CYP3A4, CYP1A2 and CYP2D6 [35]. It is worthwhile mentioning that the presented data on CYP gene expression and metabolic activity were obtained using the same cell model and, hence, provided for the first time a complete description of CYP-inhibition effect of GO in functional, differentiated hepatocytes. Continuing our investigations, we found that GST (phase-II enzyme) and ABCG2 (phase-III efflux transporter) were not affected by acute, sub-lethal GO exposure, suggesting that GO could interfere with body's xenobiotic detoxification function, preferentially at the level of phase I system, in our cell model. An impairment of cytochrome P450 system caused by GO exposure could have severe consequences for human health, such as an impaired detoxification from xenobiotics and drugs, with an increased risk of adverse side effects. Interestingly, Strojny et al. showed in HepaRG™ cells that GO (50 µg/mL) significantly downregulated CAR and PXR [35], which are nuclear receptors acting as ligand (xenobiotic)-dependent, transcription regulators of a large part of the phase-I, -II and -III executioners [44]. In upcyte® hepatocytes, CAR resulted to be un-affected by GO treatment and PXR was downregulated only at the highest concentration (80 µg/mL GO), suggesting that presumably corresponding protein levels were unaltered. Such evidence imply that GO could interfere with gene expression of CYPs via PXR- and CAR-independent molecular pathways, in our cell system. Finally, GO downregulated in a dose-dependent manner the gene expression of Albumin, which is the main plasma protein produced by liver and a typical marker of differentiated hepatocytes. It is known that Albumin production is predominantly regulated at the level of transcription and, hence, its downregulation could impair functions carried out by this protein, such as the regulation of plasma colloid osmotic pressure or the transport of endogenous molecules, ions and drugs through the blood circulation [45].

Conclusions

In conclusion, we investigated the effects of GO upon acute stimulation in upcyte® hepatocytes. Using this cell model, we were able to evaluate different aspects of the cell response to GO, as cytotoxicity, stress-related responses (apoptosis, oxidative stress and inflammatory response), along with hepatocyte-specific functions, and this large-scale approach represents the novelty of our study. In fact, some evidence have been already reported in literature but spread in different studies, using different cell

models. Moreover, upcyte® hepatocytes allowed us to study reliably the response of representative cytochromes P450 (CYP3A4, CYP2C9, CYP2B6 and CYP1A2), in terms of gene expression and metabolic activity, along with other hepatocyte markers (phase-II GST, phase-III ABCG2 and Albumin). This organic description of GO impact on hepatocyte functionality is a further new aspect about GO hepatotoxicity *in vitro*. Overall, our data raised doubts about an effective nanosafety of GO for human health, since an acute exposure of GO could have a negative impact on hepatocyte-specific functions. GO-mediated impairment of cytochrome P450 system could determine altered body's detoxification from xenobiotics and drugs, with an increased risk of adverse effects. Furthermore, Albumin downregulation could result in hypoalbuminemia, and severe consequences as edema and ascites [45]. In this framework, as long terms perspective, it would be of interest to understand if liver architecture of the hepatic lobules, when receiving similar doses, could effectively isolate hepatocytes from a direct contact with GO, preserving the hepatic functions. Moreover, one other important aspect to elucidate may be the interaction between GO and body's immune system cells (*i.e.*, Kupffer cells), which are normally resident in liver sinusoids and able to remove xenobiotics, as for instance nanomaterials, which may be carried to liver through the blood circulation [46, 47]. For these reasons, more complex 3D *in vitro* models (*e.g.*, liver organoid or liver-on-a-chip) and, ultimately, *in vivo* studies could be beneficial to clarify the effective hepatotoxicity of GO.

Methods

Materials

Second-generation upcyte® hepatocytes (donor 653-03) and Hepatocyte High Performance Medium (complete HHPM: basal medium supplemented with supplement A and L-glutamine) were purchased from upcyte® technologies GmbH (Hamburg, DE). Cell culture flasks and 96- and 24-well plates were from Corning Incorporated (Corning, NY, USA). Collagen Type I solution from rat tail, Rifampicin, Ciprofloxacin, high glucose phenol red-free Dulbecco's Modified Eagle's Medium (DMEM), Dulbecco's Phosphate Buffered Saline (DPBS), resazurin sodium salt, 7-benzyloxy-4-trifluoromethylcoumarin, 7-methoxy-4-trifluoromethylcoumarin, β-glucuronidase/arylsulfatase, Lipopolysaccharide (LPS), Triton X-100 and Staurosporine (Stau) were from Sigma Aldrich (Merck KGaA, Darmstadt, DE). Tecan Spark® multimode microplate reader was from Tecan (Männedorf, CH). CytoTox96® Non-Radioactive Cytotoxicity Assay and RealTime-Glo™ Annexin V Apoptosis and Necrosis Assay were purchased from Promega Corporation (Madison, WI, USA). Prism software was from GraphPad Software (San Diego, CA, USA). Zetasizer Nano-ZS was from Malvern Instruments (Worcestershire, UK). JSM-7500FA Field Emission Scanning Electron Microscope was from Jeol Ltd. (Akishima, JP). Pierce™ BCA Protein Assay Kit, TBS Buffer and primary antibody anti-cleaved-PARP were obtained from Thermo Fisher Scientific (Waltham, MA, USA). TRIzol™ Reagent, SuperScript™ VILO™ cDNA Synthesis Kit, custom-made qPCR primers and NuPAGE™ 4–12% Bis-Tris gel were obtained from Invitrogen (Thermo Fisher Scientific, Waltham, MA, USA). NanoDrop One^{C} was from Thermo Scientific™ (Thermo Fisher Scientific, Waltham, MA, USA). iTaq™ Universal SYBR® Green Supermix, Clarity™ Western ECL Substrate and ChemiDoc™ MP Imaging System were from Bio-Rad (Hercules, CA, USA). Applied Biosystems ViiA 7 Real-Time PCR

System was from Life Technologies (Thermo Fisher Scientific, Waltham, MA, USA). Amersham™ Protran™ 0.2 µm NC nitrocellulose blotting membrane was from GE Healthcare (Buckinghamshire, UK). Primary antibodies anti-HO-1, anti-SOD1 and anti-β-Actin, and secondary anti-rabbit and anti-mouse HRP-linked antibodies were purchased from Cell Signaling Technology (Danvers, MA, USA).

GO synthesis and characterization

Graphene oxide (GO) was kindly provided by Dr E. Vazquez (Universidad de Castilla-La Mancha, Spain). Characterization of the nanomaterial dispersed in Milli-Q® water was previously provided by Guarnieri et al. [13]. GO morphology was evaluated by scanning electron microscopy (SEM), carried out by JSM-7500FA Field Emission Scanning Electron Microscope equipped with a thermionic source. An acceleration voltage of 10.0 kV was used. GO colloidal stability was analysed as a function of concentration (4, 20 and 80 µg/mL) and incubation time (0, 2 and 24 hours at 37 °C), when dispersed in Milli-Q® water or complete HHPM. GO size distribution profiles were determined via dynamic light scattering (DLS) analysis using a Zetasizer Nano-ZS at 25 °C, even though such technique is not entirely accurate for the analysis of non-spherical particles. Five consecutive measurements were performed for each GO suspension. The number of runs per measurement, the attenuator and the optimal measurement position were set automatically. GO-free complete HHPM was used as background control. For aqueous suspensions, GO surface charge was measured via Zeta Potential (ZP) analysis using a Zetasizer Nano-ZS at 25 °C. Five consecutive measurements, with an automatically set number of runs per measurements, were taken of each GO suspension. To study particle-corona complexes, at the end of 24-hour incubation in complete HHPM, GO suspensions were centrifuged at 15’000 g for 15 minutes at 4 °C and corresponding pellets were washed three times adding a volume of Milli-Q® water equal to the initial volume [21, 22]. Particle-corona complexes were characterized via DLS and Zeta Potential, as described above. GO was endotoxin-free, as previously reported by Di Cristo et al. [14], in accordance with US Food and Drug Administration guidelines (https://www.fda.gov/regulatory-information/search-fda-guidance-documents/guidance-industry-pyrogen-and-endotoxins-testing-questions-and-answers).

Upcyte® hepatocyte culture

Second-generation human upcyte® hepatocytes (donor 653-03) were cultured following manufacturer’s indications. Upcyte® hepatocytes were seeded at the concentration of 10’000 cells/cm^2 into cell culture flasks coated with 0.1 mL/cm^2 of 50 µg/mL collagen-type I in 20 mM acetic acid, and they were cultured in complete HHPM, in incubation in a humidified atmosphere at 37 °C, with 5% CO_2. No antibiotics were added to the culture medium in order to do not alter cytochromes P450 activity. Culture medium was changed 3 times per week. Cells were expanded for 1 or 2 passages before being treated, as described below.

Cell Viability Assay

Cell viability upon GO treatment was evaluated by colorimetric resazurin reduction test. Upcyte® hepatocytes were cultured into collagen-coated, flat bottom 96-well plates (cell growth area equal to 0.3 cm^2, approximately) and, at the confluence, they were treated with different GO concentrations (final

volume equal to 75 µL per well) for 24 hours. At the end of GO treatment, stimulation media were replaced with 100 µL per well of serum-free phenol red-free high glucose DMEM, supplemented with 44 µM resazurin sodium salt, after having extensively washed with DPBS [23]. After 1-hour incubation at 37 °C in a humidified atmosphere with 5% CO_2 in the dark, resazurin solution was transferred into a clean 96-well plate and fluorescence was measured at 535 nm by Tecan Spark® reader. For each culture condition, three independent experiments were performed, each one with a technical triplicate. In each experiment, a couple of cell-free, collagen-coated wells per culture condition was incubated with the stimulation medium and used as blank value during the data analysis. The reported results are expressed as percentage values (means ± SD) compared to the control condition (set as 100%). The half maximal inhibitory concentration (IC_{50}) of GO was calculated using log(inhibitor) *vs.* normalized response curves model on Prism software.

Cytotoxicity Assay

To evaluate cell membrane damage upon GO treatment, colorimetric CytoTox96® Non-Radioactive Cytotoxicity Assay was used. Upcyte® hepatocytes were cultured into collagen-coated, flat bottom 96-well plates (cell growth area equal to 0.3 cm^2, approximately). At the confluence, cells were treated with different GO concentrations (final volume equal to 75 µL per well) for 24 hours. As a positive control, confluent cells were treated with complete medium supplemented with 0.03% Triton X-100 for 24 hours. At the end of stimulation, conditioned media were collected, centrifuged at 15'000 g for 15 minutes at 4 °C, and analysed following manufacturer's instructions. For each culture condition, three independent experiments were performed, each one with a technical triplicate. In each experiment, a couple of cell-free, collagen-coated wells per culture condition was incubated with the stimulation medium and used as blank value during the data analysis. The results are expressed as percentage net increase of the absorbance (means ± SD) compared to the positive control (set as 100%), after having subtracted the basal value of the control condition (set as 0%).

Apoptosis and Necrosis Assay

To assess the induction of apoptosis and necrosis, RealTime-Glo™ Annexin V Apoptosis and Necrosis Assay was used, according to manufacturer's instructions. Upcyte® hepatocytes were cultured into collagen-coated, flat bottom 96-well plates (cell growth area equal to 0.3 cm^2, approximately). At the confluence, cells were treated for 24 hours with complete medium supplemented with GO at different concentrations, in the presence of detection reagent (final volume equal to 75 µL per well). As a positive control, confluent cells were treated for 24 hours with 0.5 µM Staurosporine (Stau), diluted in the same incubation medium. After 3, 6 and 24 hours of incubation, luminescence and fluorescence (at 530 nm) were measured by Tecan Spark® reader for the induction of apoptosis and necrosis, respectively. For each culture condition, three independent experiments were performed, each one with a technical triplicate. In each experiment, a couple of cell-free, collagen-coated wells per culture condition was incubated with the incubation medium and used as blank value during the data analysis. Apoptosis data are expressed as n-fold increase over the control conditions (means ± SD) for each incubation time.

Necrosis results are expressed as net increase of absorbance for each condition (means ± SD), after having subtracted the basal value of the control cells obtained after 3 hours of incubation (set as 0 a.u.).

Reverse Transcription and Quantitative Real-Time PCR

For gene expression analysis of GO-treated cells, upcyte® hepatocytes were cultured into collagen-coated, flat bottom 24-well plates (cell growth area equal to 2.0 cm^2, approximately) and, at the confluence, they were treated with different GO concentrations (final volume equal to 500 µL per well) for 24 hours. At the end of stimulation, cells were extensively washed with DPBS and incubated with TRIzol™ Reagent (500 µL per well) at -80 °C for at least one night. Total RNA was isolated according to manufacturer's instructions. RNA yield was determined measuring absorbance at 260 nm with NanoDrop One^C, while RNA purity was examined considering A260/A280 and A260/A230 ratios. Total RNA (2 µg/sample in 20 µL of total volume reaction) was reverse-transcribed to first-strand cDNA by SuperScript™ VILO™ cDNA Synthesis Kit, following manufacturer's instructions. Transcript levels of target genes were measured by quantitative Real-Time PCR (qPCR) using iTaq™ Universal SYBR® Green Supermix, on Applied Biosystems ViiA 7 Real-Time PCR System. Custom-made primer sequences, temperatures of annealing, corresponding amplicon sizes and qPCR efficiencies are reported in **Table 1** (*Supplementary Material*). The gene expression of GAPDH was used as endogenous control (reference gene). For each primer pair, melting curve analysis was carried out in order to verify the production of a single amplicon and, consequently, primer specificity. Transcript levels were calculated using Pfaffl's model for relative quantification [24]. In each run, samples were assayed in technical triplicate. The results are expressed as the average of three independent experiments, with the relative SD values.

Western blot

To evaluate GO effects on apoptosis and oxidative stress, protein content from GO-treated upcyte® hepatocytes was analysed by western blot. In particular, proteins were isolated starting from the same homogenates used for RNA isolation as described by Chomczynski [25]. The protein content was quantified by Pierce™ BCA Protein Assay Kit, following manufacturer's instructions. Electrophoresis was performed loading 20 µg of total protein per sample on NuPAGE™ 4–12% Bis-Tris gel, under reducing conditions. Proteins were transferred to an Amersham™ Protran™ 0.2 µm NC nitrocellulose blotting membrane. The blot was blocked with 5% non-fat milk in TBS Buffer, supplemented with 0.1% Tween 20 (T-TBS), for at least 1 hour at room temperature and then probed with primary antibodies raised against cleaved-PARP (1:1'000), HO-1 (1:1'000), SOD1 (1:500) or β-Actin (1:1'000), overnight in a cold room. β-Actin was considered as internal control. The blot was extensively washed with T-TBS and incubated with secondary anti-rabbit (1:15'000) or anti-mouse (1:10'000) HRP-linked IgG antibodies, for 1 hour at room temperature. Then, blot was washed with T-TBS and incubated with Clarity™ Western ECL Substrate, following manufacturer's instructions. The blot image was acquired by ChemiDoc™ MP Imaging System. Each considered marker was analysed by western blot in three independent experiments. The densitometric analysis was performed by quantifying band densities by Fiji software (http://fiji.sc [26]). The reported results are expressed as n-fold increase over the control condition (means ± SD).

Cytochrome P450 activity assay

To evaluate the enzymatic activity of CYP3A4 and CYP2C9 in GO-treated cells, the conversion of 7-benzyloxy-4-trifluoromethylcoumarin (BFC) or 7-methoxy-4-trifluoromethylcoumarin (MFC) to 7-hydroxy-4-trifluoromethylcoumarin (HFC) was monitored as described by Donato et al. [27], with some modifications. Upcyte® hepatocytes were seeded into collagen-coated, flat bottom 96-well plates (cell growth area equal to 0.3 cm^2, approximately) and, at the confluence, they were treated with different GO concentrations for 24 hours (final volume equal to 75 µL per well). As positive and negative controls, confluent cells were treated for 72 hours with complete medium supplemented with 50 µM Rifampicin or 100 µM Ciprofloxacin, respectively, changing the stimulation medium every day, after an early wash with DPBS [28, 29]. At the end of treatments, cells were washed with DPBS and they were incubated with 100 µL per well of 100 µM BFC or 150 µM MFC in incubation medium (1 mM Na_2HPO_4, 137 mM NaCl, 5 mM KCl, 0.5 mM $MgCl_2$, 2 mM $CaCl_2$, 10 mM glucose, 10 mM Hepes; pH 7.4 buffered solution) for 2 hours at 37 °C, in a humidified atmosphere with 5% CO_2. After the incubation with BFC or MFC, the supernatant was collected, diluted 1:1 (v/v) with β-glucuronidase/arylsulfatase (150 Fishman units/mL and 1200 Roy units/mL, respectively) and incubated for 2 hours at 37 °C. At the end of this step, the reaction mixture was diluted 1:1 (v/v) with the quenching solution (0.25 M Tris in 60% acetonitrile). Finally, the formation of the fluorescent HFC metabolite was quantified at the wavelength of 410 nm (excitation) and 510 nm (emission) by Tecan Spark® reader. Each culture condition was assayed in technical triplicate, in three independent experiments. In each experiment, a couple of cell-free, collagen-coated wells per culture condition was incubated with the stimulation medium and used as blank value during the data analysis. The reported results are expressed as percentage values (means ± SD) over the control condition (set as 100%).

Statistical analysis

Statistical analysis was run on Prism software. Ordinary one-way ANOVA was performed for cell viability assay, cytotoxicity assay, apoptosis assay, qPCR analysis, western blot analysis and cytochrome P450 activity assay. If ANOVA detected statistically significant differences within the data set, Dunnett's multiple comparisons test (cytotoxicity assay, apoptosis assay, qPCR analysis and cytochrome P450 activity assay) or Tukey's multiple comparisons test (cell viability assay) were used to calculate significant differences. Two-way ANOVA was used for necrosis assay, with Sidak's multiple comparisons test. Unpaired t-Test was used to calculate significant differences within data sets obtained by qPCR analysis or cytochrome P450 activity assay between the control condition and the drug-treated cells. GO IC_{50} was calculated using log(inhibitor) *vs.* normalized response curves model. Correlation between cell viability and cytotoxicity data and between relative gene expression and metabolic activity data of CYP3A4 and CYP2C9 was calculated using a linear regression. All tests were run setting a confidence interval of 95%. When $p < 0.05$, differences were considered statistically significant. All data are presented as means ± standard deviations (SD) of three independent experiments.

List Of Abbreviations

GO, Graphene Oxide; PHH, Primary Human Hepatocytes; CYP450, Cytochromes P450; HHPM, Hepatocyte High Performance Medium; DMEM, Dulbecco's Modified Eagle's Medium; DPBS, Dulbecco's Phosphate

Buffered Saline; LPS, Lipopolysaccharide; LDH, Lactate Dehydrogenase; Stau, Staurosporine; PtdSer, Phosphatidylserine; BFC, 7-benzyloxy-4-trifluoromethylcoumarin; MFC, 7-methoxy-4-trifluoromethylcoumarin; HFC, 7-hydroxy-4-trifluoromethylcoumarin; PXR, Pregnane X Receptor; CAR, Constitutive Androstane Receptor; TNFα, Tumour Necrosis Factor Alfa; IL-1β, Interleukin 1 Beta, IL-6, Interleukin 6; IL-8, Interleukin 8; GST, Glutathione S-Transferase; ABCG2, ATP Binding Cassette Subfamily G Member 2; TGFβ1, Transforming Growth Factor Beta 1; SEM, Scanning Electron Microscopy; DLS, Dynamic Light Scattering; ZP, Zeta Potential; IC_{50}, half maximal inhibitory concentration.

Declarations

Availability of data and materials

The datasets used and/or analyzed during the current study are available from the corresponding author on reasonable request.

Acknowledgements

The authors would like to thank Dr E. Vazquez (Universidad de Castilla-La Mancha, Spain) for GO purification, Dr D. Cavallo (INAIL), Dr L. Ursini (INAIL) and Professor S. Iavicoli (INAIL) for the fruitful discussions. The authors also thank Dr D. Debellis for the technical assistance with SEM images and Dr B. Grimaldi (IIT) and Dr L. Di Cristo (IIT) for their beneficial advises.

Funding

This work has partially received funding from Istituto Italiano Nazionale per l'Assicurazione contro gli Infortuni sul Lavoro (INAIL) (NanoKEY_EPTR0003).

Authors' information

Drug Discovery and Development Department, Istituto Italiano di Tecnologia, via Morego 30, 16136, Genoa, Italy (AR, RS and SS)

AUTHORS' CONTRIBUTIONS

AR and RS equally contributed to conception and design of the study, experiments, data analysis and manuscript writing. SS contributed to conception and design of the study, data analysis, manuscript writing and financial support.

CORRESPONDING AUTHOR

Stefania Sabella (stefania.sabella@iit.it)

Ethics declarations

Ethics approval and consent to participate

Not applicable.

CONSENT FOR PUBLICATION

All authors have given their consent for publication of this manuscript.

COMPETING INTERESTS

The authors declare that they have no competing interests.

References

1. Novoselov KS. Electric Field Effect in Atomically Thin Carbon Films. Science (80-) [Internet]. 2004;306:666–9. Available from: http://www.sciencemag.org/cgi/doi/10.1126/science.1102896
2. Liu J, Cui L, Losic D. Graphene and graphene oxide as new nanocarriers for drug delivery applications. Acta Biomater [Internet]. 2013;9:9243–57. Available from: https://linkinghub.elsevier.com/retrieve/pii/S174270611300408X
3. Zhao H, Ding R, Zhao X, Li Y, Qu L, Pei H, et al. Graphene-based nanomaterials for drug and/or gene delivery, bioimaging, and tissue engineering. Drug Discov Today [Internet]. 2017;22:1302–17. Available from: https://linkinghub.elsevier.com/retrieve/pii/S1359644617301733
4. Loh KP, Bao Q, Eda G, Chhowalla M. Graphene oxide as a chemically tunable platform for optical applications. Nat Chem [Internet]. 2010;2:1015–24. Available from: http://www.nature.com/articles/nchem.907
5. Chen D, Feng H, Li J. Graphene Oxide: Preparation, Functionalization, and Electrochemical Applications. Chem Rev [Internet]. 2012;112:6027–53. Available from: https://pubs.acs.org/doi/10.1021/cr300115g
6. Fadeel B, Bussy C, Merino S, Vázquez E, Flahaut E, Mouchet F, et al. Safety Assessment of Graphene-Based Materials: Focus on Human Health and the Environment. ACS Nano [Internet]. 2018;12:10582–620. Available from: https://pubs.acs.org/doi/10.1021/acsnano.8b04758
7. Jasim DA, Ménard-Moyon C, Bégin D, Bianco A, Kostarelos K. Tissue distribution and urinary excretion of intravenously administered chemically functionalized graphene oxide sheets. Chem Sci. 2015;6:3952–64.
8. Li B, Zhang X, Yang J, Zhang Y, Li W, Fan C, et al. Influence of polyethylene glycol coating on biodistribution and toxicity of nanoscale graphene oxide in mice after intravenous injection. Int J Nanomedicine [Internet]. 2014;4697. Available from: http://www.dovepress.com/influence-of-polyethylene-glycol-coating-onnbspbiodistribution-and-tox-peer-reviewed-article-IJN
9. Qu G, Wang X, Liu Q, Liu R, Yin N, Ma J, et al. The ex vivo and in vivo biological performances of graphene oxide and the impact of surfactant on graphene oxide's biocompatibility. J Environ Sci

[Internet]. 2013;25:873–81. Available from: https://linkinghub.elsevier.com/retrieve/pii/S1001074212602526

10. Zhang Y, Ma C, Wang Z, Zhou Q, Sun S, Ma P, et al. Large-sized graphene oxide synergistically enhances parenchymal hepatocyte IL-6 expression monitored by dynamic imaging. Nanoscale. Royal Society of Chemistry; 2020;12:8147–58.
11. Kanakia S, Toussaint JD, Mullick Chowdhury S, Tembulkar T, Lee S, Jiang YP, et al. Dose ranging, expanded acute toxicity and safety pharmacology studies for intravenously administered functionalized graphene nanoparticle formulations. Biomaterials [Internet]. Elsevier Ltd; 2014;35:7022–31. Available from: http://dx.doi.org/10.1016/j.biomaterials.2014.04.066
12. Kurantowicz N, Strojny B, Sawosz E, Jaworski S, Kutwin M, Grodzik M, et al. Biodistribution of a High Dose of Diamond, Graphite, and Graphene Oxide Nanoparticles After Multiple Intraperitoneal Injections in Rats. Nanoscale Res Lett. 2015;10.
13. Guarnieri D, Sánchez-Moreno P, Del Rio Castillo AE, Bonaccorso F, Gatto F, Bardi G, et al. Biotransformation and Biological Interaction of Graphene and Graphene Oxide during Simulated Oral Ingestion. Small. 2018;14:1–11.
14. Di Cristo L, Grimaldi B, Catelani T, Vázquez E, Pompa PP, Sabella S. Repeated exposure to aerosolized graphene oxide mediates autophagy inhibition and inflammation in a three-dimensional human airway model. Mater Today Bio [Internet]. 2020;6:100050. Available from: https://linkinghub.elsevier.com/retrieve/pii/S2590006420300107
15. Chatterjee N, Eom H-J, Choi J. A systems toxicology approach to the surface functionality control of graphene–cell interactions. Biomaterials [Internet]. 2014;35:1109–27. Available from: https://linkinghub.elsevier.com/retrieve/pii/S0142961213012088
16. Liu S, Jiang W, Wu B, Yu J, Yu H, Zhang X-X, et al. Low levels of graphene and graphene oxide inhibit cellular xenobiotic defense system mediated by efflux transporters. Nanotoxicology [Internet]. 2016;10:597–606. Available from: http://www.tandfonline.com/doi/full/10.3109/17435390.2015.1104739
17. Tolosa L, Gómez-Lechón MJ, López S, Guzmán C, Castell J V., Donato MT, et al. Human upcyte hepatocytes: Characterization of the hepatic phenotype and evaluation for acute and long-term hepatotoxicity routine testing. Toxicol Sci. 2016;152:214–29.
18. Feng M, Kong R, Pan Y. The breakthrough in primary human hepatocytes in vitro expansion. Cancer Biol Med [Internet]. 2019;16:1–3. Available from: http://www.ncbi.nlm.nih.gov/pubmed/31119041
19. Levy G, Bomze D, Heinz S, Ramachandran SD, Noerenberg A, Cohen M, et al. Long-term culture and expansion of primary human hepatocytes. Nat Biotechnol [Internet]. Nature Publishing Group; 2015;33:1264–71. Available from: http://dx.doi.org/10.1038/nbt.3377
20. Burkard A, Dähn C, Heinz S, Zutavern A, Sonntag-Buck V, Maltman D, et al. Generation of proliferating human hepatocytes using upcyte® technology: Characterisation and applications in induction and cytotoxicity assays. Xenobiotica. 2012;42:939–56.

21. Magrì D, Sánchez-Moreno P, Caputo G, Gatto F, Veronesi M, Bardi G, et al. Laser Ablation as a Versatile Tool To Mimic Polyethylene Terephthalate Nanoplastic Pollutants: Characterization and Toxicology Assessment. ACS Nano [Internet]. 2018;12:7690–700. Available from: https://pubs.acs.org/doi/10.1021/acsnano.8b01331
22. Maiorano G, Sabella S, Sorce B, Brunetti V, Malvindi MA, Cingolani R, et al. Effects of Cell Culture Media on the Dynamic Formation of Protein–Nanoparticle Complexes and Influence on the Cellular Response. ACS Nano [Internet]. 2010;4:7481–91. Available from: https://pubs.acs.org/doi/10.1021/nn101557e
23. O'Brien J, Wilson I, Orton T, Pognan F. Investigation of the Alamar Blue (resazurin) fluorescent dye for the assessment of mammalian cell cytotoxicity. Eur J Biochem [Internet]. 2000;267:5421–6. Available from: http://doi.wiley.com/10.1046/j.1432-1327.2000.01606.x
24. Pfaffl MW. A new mathematical model for relative quantification in real-time RT-PCR. Nucleic Acids Res [Internet]. 2001;29:45e – 45. Available from: https://academic.oup.com/nar/article-lookup/doi/10.1093/nar/29.9.e45
25. Chomczynski P. A reagent for the single-step simultaneous isolation of RNA, DNA and proteins from cell and tissue samples. Biotechniques. 1993;15:532–7.
26. Schindelin J, Arganda-Carreras I, Frise E, Kaynig V, Longair M, Pietzsch T, et al. Fiji: an open-source platform for biological-image analysis. Nat Methods [Internet]. 2012;9:676–82. Available from: http://www.nature.com/articles/nmeth.2019
27. Donato MT, Jiménez N, Castell J V., Gómez-Lechón MJ. Fluorescence-based assays for screening nine cytochrome P450 (P450) activities in intact cells expressing individual human P450 enzymes. Drug Metab Dispos. 2004;32:699–706.
28. Fahmi OA, Boldt S, Kish M, Obach RS, Tremaine LM. Prediction Of Drug-Drug Interactions From In Vitro Induction Data. Drug Metab Dispos [Internet]. 2008;36:1971–4. Available from: http://dmd.aspetjournals.org/lookup/doi/10.1124/dmd.108.021907
29. Bjornsson TD, Callaghan JT, Einolf HJ, Fischer V, Gan L, Grimm S, et al. The conduct of in vitro and in vivo drug-drug interaction studies: a Pharmaceutical Research and Manufacturers of America (PhRMA) perspective. Drug Metab Dispos [Internet]. 2003;31:815–32. Available from: http://dmd.aspetjournals.org/lookup/doi/10.1124/dmd.31.7.815
30. Di Cristo L, Carthy SM, Paton K, Movia D, Prina-Mello A. Interplay between oxidative stress and endoplasmic reticulum stress mediated- autophagy in unfunctionalised few-layer graphene-exposed macrophages. 2D Mater. IOP Publishing; 2018;5.
31. Ramachandran SD, Vivarès A, Klieber S, Hewitt NJ, Muenst B, Heinz S, et al. Applicability of second-generation upcyte ® human hepatocytes for use in CYP inhibition and induction studies. Pharmacol Res Perspect [Internet]. 2015;3:e00161. Available from: http://doi.wiley.com/10.1002/prp2.161
32. Park MVDZ, Bleeker EAJ, Brand W, Cassee FR, van Elk M, Gosens I, et al. Considerations for Safe Innovation: The Case of Graphene. ACS Nano [Internet]. 2017;11:9574–93. Available from: https://pubs.acs.org/doi/10.1021/acsnano.7b04120

33. Anthérieu S, Chesné C, Li R, Guguen-Guillouzo C, Guillouzo A. Optimization of the HepaRG cell model for drug metabolism and toxicity studies. Toxicol Vitr [Internet]. 2012;26:1278–85. Available from: https://linkinghub.elsevier.com/retrieve/pii/S0887233312001415
34. Nelson LJ, Morgan K, Treskes P, Samuel K, Henderson CJ, LeBled C, et al. Human Hepatic HepaRG Cells Maintain an Organotypic Phenotype with High Intrinsic CYP450 Activity/Metabolism and Significantly Outperform Standard HepG2/C3A Cells for Pharmaceutical and Therapeutic Applications. Basic Clin Pharmacol Toxicol. 2017;120:30–7.
35. Strojny B, Sawosz E, Grodzik M, Jaworski S, Szczepaniak J, Sosnowska M, et al. Nanostructures of diamond, graphene oxide and graphite inhibit CYP1A2, CYP2D6 and CYP3A4 enzymes and downregulate their genes in liver cells. Int J Nanomedicine. 2018;13:8561–75.
36. Zheng T, Gao Y, Deng X, Liu H, Liu J, Liu R, et al. Comparisons between Graphene Oxide and Graphdiyne Oxide in Physicochemistry Biology and Cytotoxicity. ACS Appl Mater Interfaces [Internet]. 2018;10:32946–54. Available from: https://pubs.acs.org/doi/10.1021/acsami.8b06804
37. Segawa K, Nagata S. An Apoptotic 'Eat Me' Signal: Phosphatidylserine Exposure. Trends Cell Biol [Internet]. 2015;25:639–50. Available from: https://linkinghub.elsevier.com/retrieve/pii/S0962892415001531
38. Nicholson DW, Ali A, Thornberry NA, Vaillancourt JP, Ding CK, Gallant M, et al. Identification and inhibition of the ICE/CED-3 protease necessary for mammalian apoptosis. Nature [Internet]. 1995;376:37–43. Available from: http://www.nature.com/articles/376037a0
39. Tewari M, Quan LT, O'Rourke K, Desnoyers S, Zeng Z, Beidler DR, et al. Yama/CPP32β, a mammalian homolog of CED-3, is a CrmA-inhibitable protease that cleaves the death substrate poly(ADP-ribose) polymerase. Cell [Internet]. 1995;81:801–9. Available from: https://linkinghub.elsevier.com/retrieve/pii/0092867495905413
40. Lammel T, Boisseaux P, Fernández-Cruz M-L, Navas JM. Internalization and cytotoxicity of graphene oxide and carboxyl graphene nanoplatelets in the human hepatocellular carcinoma cell line Hep G2. Part Fibre Toxicol [Internet]. 2013;10:27. Available from: http://particleandfibretoxicology.biomedcentral.com/articles/10.1186/1743-8977-10-27
41. Lee SW, Park HJ, Van Kaer L, Hong S, Hong S. Graphene oxide polarizes iNKT cells for production of TGFβ and attenuates inflammation in an iNKT cell-mediated sepsis model. Sci Rep [Internet]. 2018;8:10081. Available from: http://www.nature.com/articles/s41598-018-28396-9
42. Han J, Kim YS, Lim MY, Kim HY, Kong S, Kang M, et al. Dual Roles of Graphene Oxide to Attenuate Inflammation and Elicit Timely Polarization of Macrophage Phenotypes for Cardiac Repair. ACS Nano. 2018;12:1959–77.
43. Anzenbacher P, Anzenbacherová E. Cytochromes P450 and metabolism of xenobiotics. Cell Mol Life Sci [Internet]. 2001;58:737–47. Available from: http://link.springer.com/10.1007/PL00000897
44. Evans RM, Mangelsdorf DJ. Nuclear Receptors, RXR, and the Big Bang. Cell [Internet]. 2014;157:255–66. Available from: https://linkinghub.elsevier.com/retrieve/pii/S0092867414003468

45. Chojkier M. Inhibition of albumin synthesis in chronic diseases: molecular mechanisms. J Clin Gastroenterol [Internet]. 2005;39:S143-6. Available from: http://www.ncbi.nlm.nih.gov/pubmed/15758650
46. Tsoi KM, Macparland SA, Ma XZ, Spetzler VN, Echeverri J, Ouyang B, et al. Mechanism of hard-nanomaterial clearance by the liver. Nat Mater. 2016;15:1212–21.
47. Zhang Y-N, Poon W, Tavares AJ, McGilvray ID, Chan WCW. Nanoparticle–liver interactions: Cellular uptake and hepatobiliary elimination. J Control Release [Internet]. 2016;240:332–48. Available from: https://linkinghub.elsevier.com/retrieve/pii/S0168365916300190

Figures

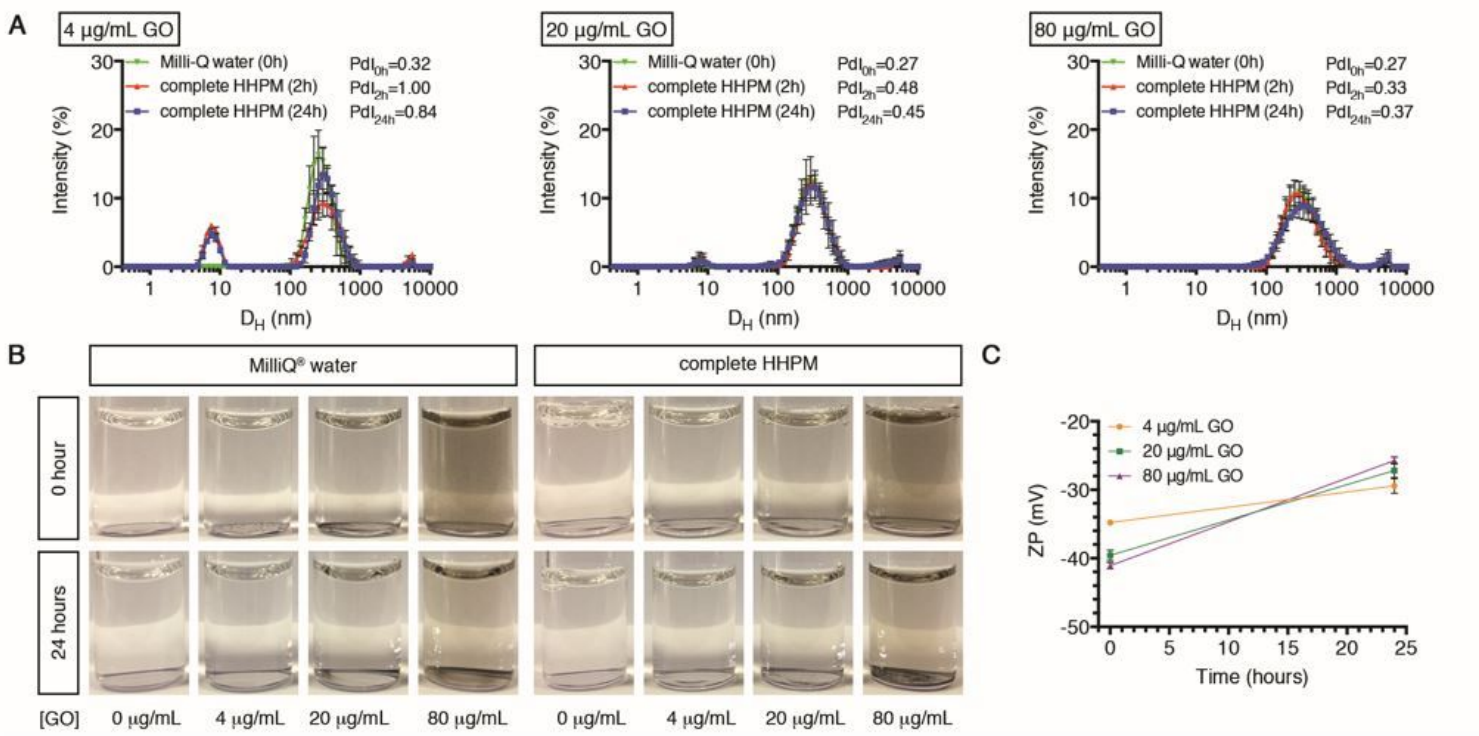

Figure 1

Characterization of GO dispersed in Milli-Q® water or in complete HHPM. (A) Size distribution profiles by DLS analysis of GO dispersed in Milli-Q® water (green curves) and in complete HHPM for 2 hours (red curves) or 24 hours (blue curves). Measurements refer to three GO concentrations. (B) Representative images of GO suspensions in Milli-Q® water and in complete HHPM at three GO concentrations after 0 or 24 hours of incubation. (C) Surface charge by Zeta Potential analysis of GO in Milli-Q® water and of particle-corona complexes dispersed in Milli-Q® water (such complexes are derived from 24-hour incubation of GO in complete HHPM as reported by Maiorano et al. [22]).

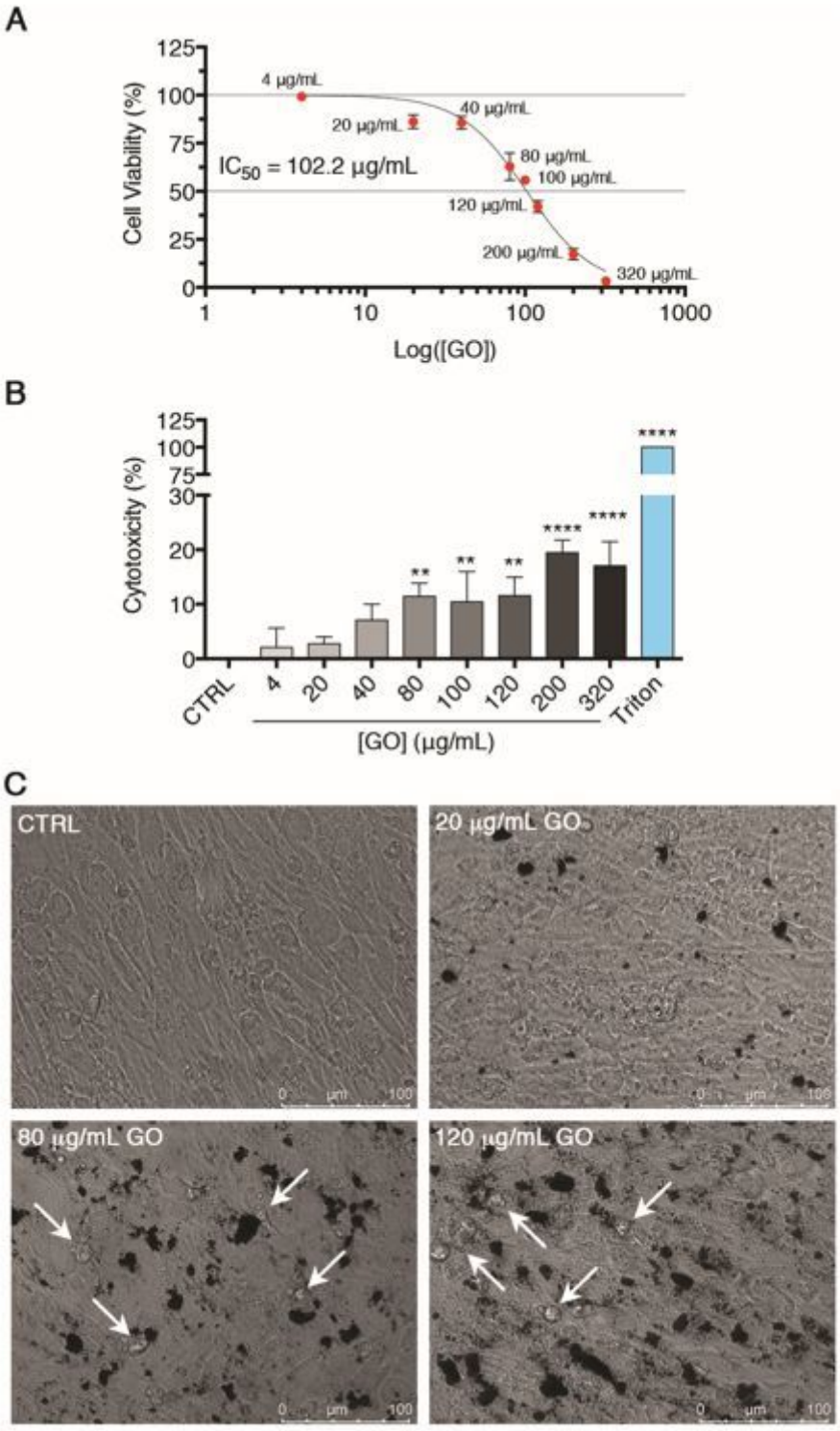

Figure 2

Confluent upcyte® hepatocyte cultures treated with increasing GO concentrations for 24 hours. (A) Cell viability of GO-treated cells evaluated by resazurin reduction assay. Results are expressed as percentage values compared to the control conditions (indicated as CTRL). Results represent means ± SD of three independent experiments. The half maximal inhibitory concentration (IC50) of GO was calculated using log(inhibitor) vs. normalized response curves model (R2 = 0.98). (B) Cell membrane damage by

cytotoxicity assay in GO-treated cells. ‘Triton’ refers to the positive control, i.e. cells treated with 0.03% Triton X-100 for 24 hours, while ‘CTRL’ represents un-treated cells. Results are expressed as percentage values compared to Triton (set as 100%), after having removed the basal value of CTRL (set as 0%). Results were obtained from three independent experiments (means ± SD). The symbols ‘**’ and ‘****’ refer to $p \leq 0.0038$ and $p < 0.0001$ respectively, calculated versus CTRL (ordinary one-way ANOVA). (C) Representative morphology of GO-treated and CTRL cells at the end of stimulation by optical microscopy. White arrows indicate morphologically altered cells. All the images are 40x magnifications (scale bar = 100 µm).

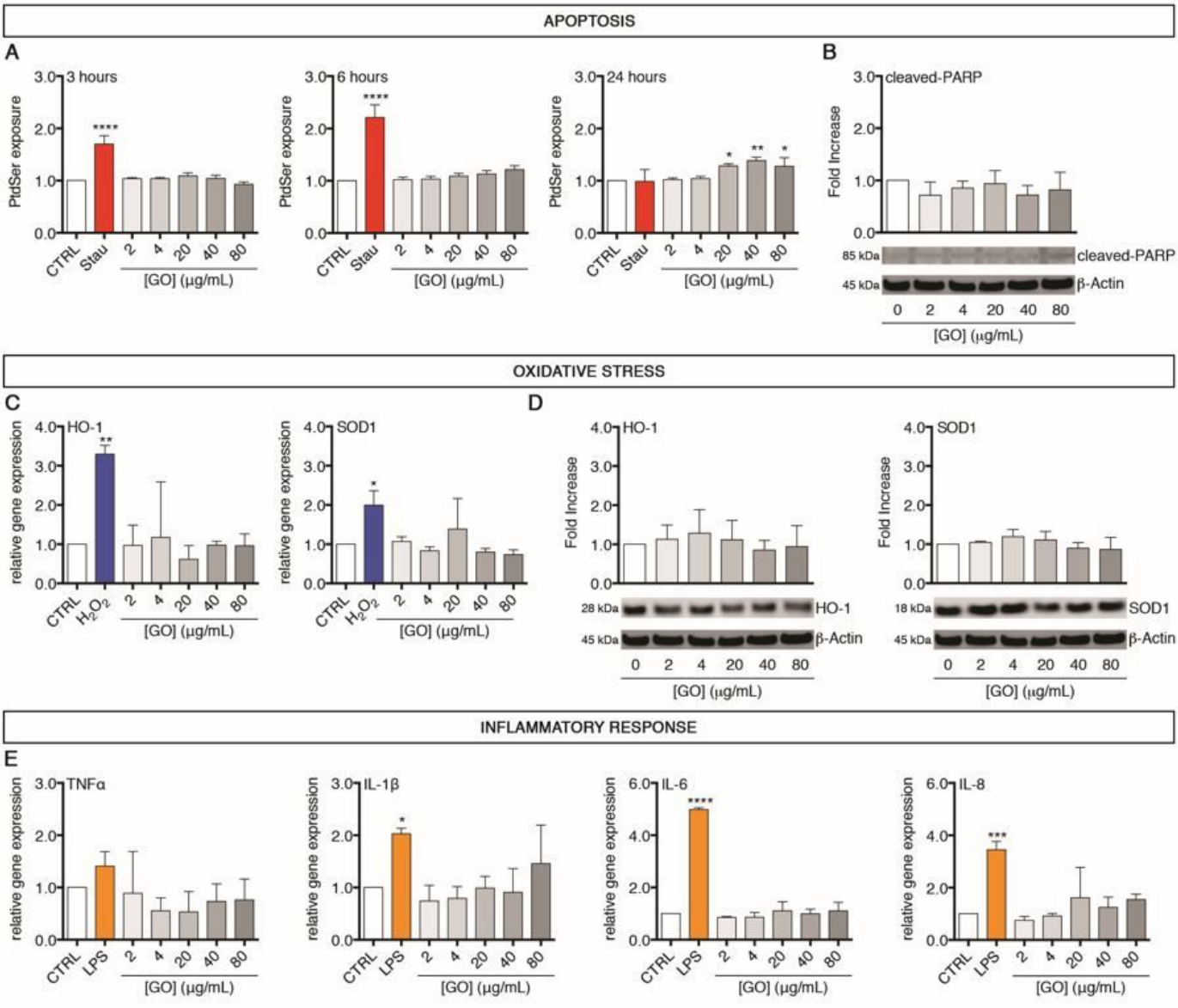

Figure 3

Twenty-four-hour exposure of GO induces early weak apoptosis but not oxidative stress nor inflammation in upcyte® hepatocytes treated at sub-lethal concentrations. (A) Temporal exposure of Phosphatidylserine (PtdSer) in GO-treated cells evaluated at different time points (3, 6 and 24 hours) by apoptosis assay. ‘Stau’ refers to the positive control, represented by cells treated with 0.5 µM

Staurosporine for 24 hours. Results are expressed as n-fold increase over the control condition (indicated as CTRL) for each incubation time. Results represent means ± SD of three independent experiments. The symbols '*', '**' and '****' refer to $p \leq 0.0429$, $p = 0.0043$ and $p < 0.0001$, respectively, calculated versus CTRL (ordinary one-way ANOVA). (B) Protein levels of cleaved-PARP in GO-treated cells in comparison to CTRL, assessed by western blot. Densitometric analysis of three blots derived from independent experiments (means ± SD; upper panel) and a representative blot (lower panel) are reported. β-Actin was used as internal control to normalize densitometric values of all culture conditions. (C) Relative gene expression of cellular antioxidants HO-1 (left) and SOD1 (right) in GO-treated cells versus CTRL, analysed by qPCR. 'H2O2' refers to the positive control, represented by cells treated with 400 μM H2O2 overnight. Results are expressed as means ± SD values of three independent experiments. The symbols '*' and '**' refer to $p = 0.0269$ and $p = 0.0094$, respectively, calculated versus CTRL (ordinary one-way ANOVA). (D) Protein levels of HO-1 (left) and SOD1 (right) in GO-treated cells in comparison to CTRL, assessed by western blot. For each marker, densitometric analysis of three blots derived from independent experiments (means ± SD; upper panel) and a representative blot (lower panel) are reported. β-Actin was used as internal control to normalize densitometric values of all culture conditions. (E) Relative gene expression of four inflammation mediators (TNFα, IL-1β, IL-6 and IL-8) in GO-treated cells versus CTRL, analysed by qPCR. 'LPS' refers to the positive control, represented by cells treated with 100 μg/mL LPS overnight. Results are expressed as means ± SD values of three independent experiments. The symbols '*', '***' and '****' refer to $p = 0.0482$, $p = 0.0001$ and $p < 0.0001$ respectively, calculated versus CTRL (ordinary one-way ANOVA).

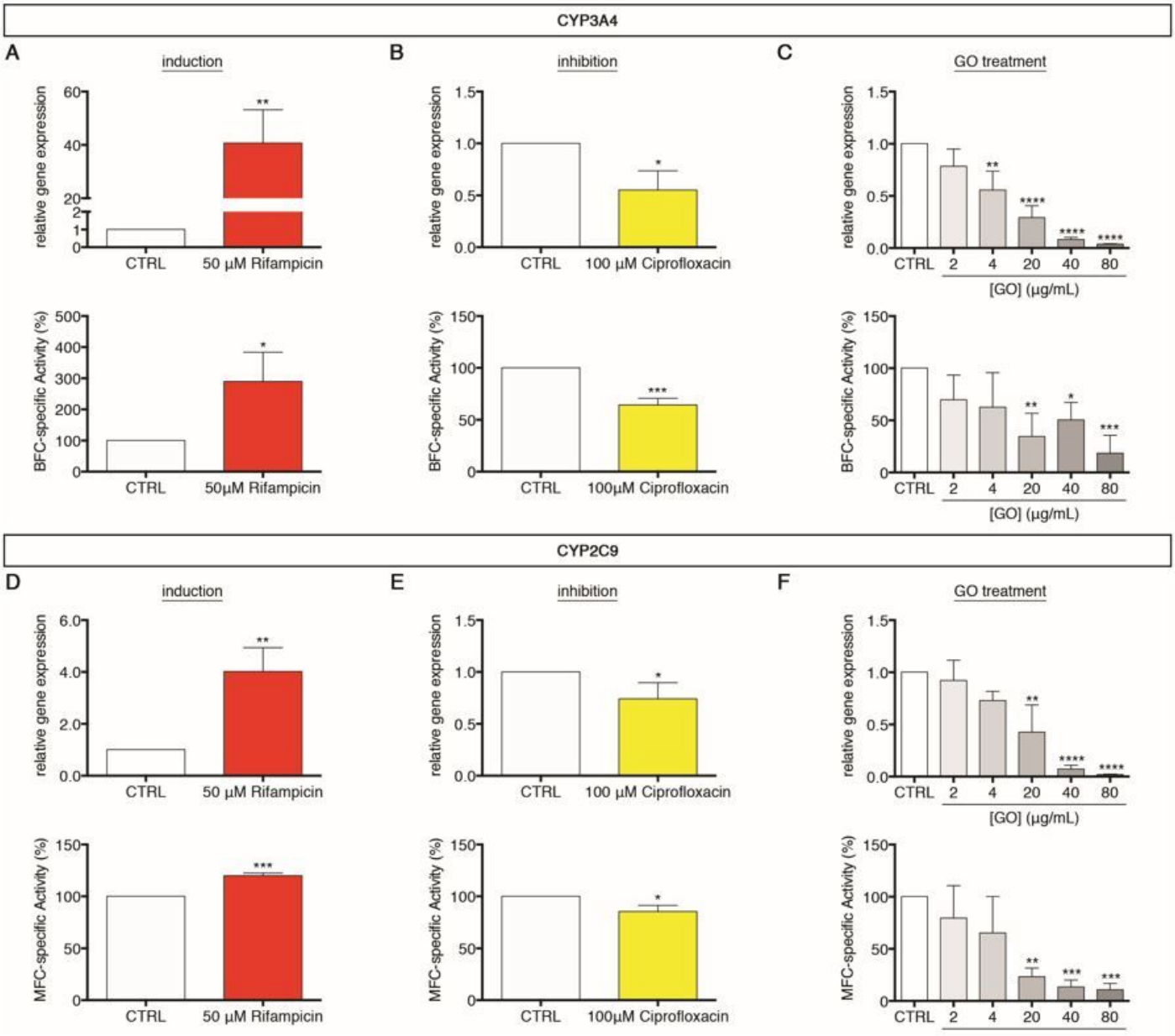

Figure 4

Modulation of the cytochrome P450 system in upcyte® hepatocytes upon sub-lethal GO exposure. (A, B) Relative gene expression and BFC-specific metabolic activity of CYP3A4 in cells treated daily up to 72 hours with 50 µM Rifampicin (A) or 100 µM Ciprofloxacin (B) in comparison to un-treated cells (indicated as CTRL). Results are expressed as means ± SD values of three independent experiments. The symbols '*', '**' and '***' refer to $p \leq 0.0247$, $p = 0.0052$ and $p = 0.0006$, respectively, calculated versus CTRL (unpaired t-Test). (C) Relative gene expression and BFC-specific metabolic activity of CYP3A4 in GO-treated cells in comparison to CTRL. Results are expressed as means ± SD values of three independent experiments. The symbols '*', '**', '***' and '****' refer to $p = 0.0164$, $p \leq 0.0017$, $p = 0.0002$ and $p < 0.0001$ respectively, calculated versus CTRL (ordinary one-way ANOVA). (D, E) Relative gene expression and MFC-specific metabolic activity of CYP2C9 in cells treated daily up to 72 hours with 50 µM Rifampicin (D) or 100 µM Ciprofloxacin (E) in comparison to CTRL. Results are expressed as means ± SD values of three

independent experiments. The symbols '*', '**' and '***' refer to p ≤ 0.0444, p = 0.0047 and p = 0.0001, respectively, calculated versus CTRL (unpaired t-Test). (F) Relative gene expression and MFC-specific metabolic activity of CYP2C9 in GO-treated cells in comparison to CTRL. Results are expressed as means ± SD values of three independent experiments. The symbols '**', '***' and '****' refer to p ≤ 0.0019, p ≤ 0.0007 and p < 0.0001 respectively, calculated versus CTRL (ordinary one-way ANOVA).

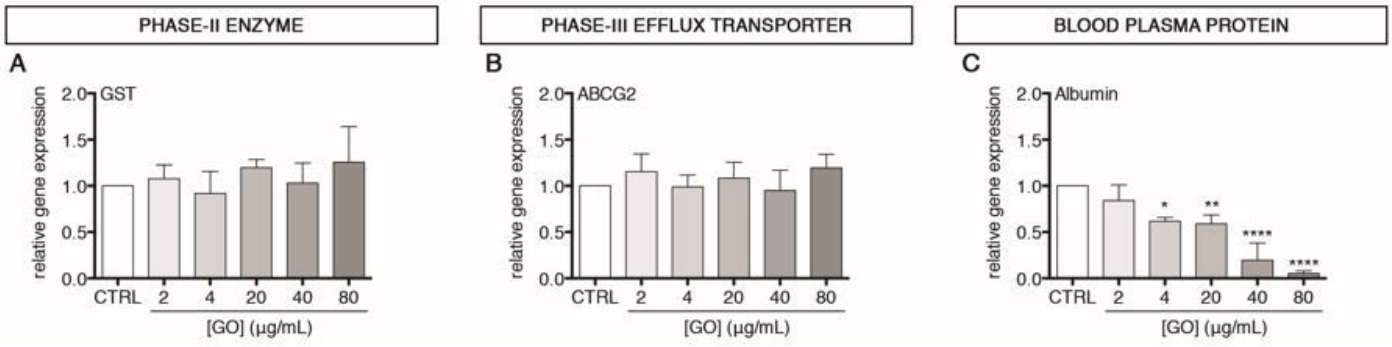

Figure 5

Modulation of upcyte® hepatocyte-specific functions after sub-lethal GO treatment. (A-C) Relative gene expression of GST (A), ABCG2 (B) and Albumin (C) in GO-treated cells versus un-treated cells (indicated as CTRL). Results are expressed as means ± SD values of three independent experiments. The symbols '*', '**' and '****' refer to p = 0.0155, p = 0.0046 and p < 0.0001, respectively, calculated versus CTRL (ordinary one-way ANOVA).

Supplementary Files

This is a list of supplementary files associated with this preprint. Click to download.

- SupplementaryMaterialUpcyteHepatocytes010121.docx